Status and Prospects of AlN Templates on Sapphire for Ultraviolet Light-Emitting Diodes

Sylvia Hagedorn, Sebastian Walde, Arne Knauer, Norman Susilo, Daniel Pacak, Leonardo Cancellara, Carsten Netzel, Anna Mogilatenko, Carsten Hartmann, Tim Wernicke, Michael Kneissl, and Markus Weyers*

Herein, the scope is to provide an overview on the current status of AlN/sapphire templates for ultraviolet B (UVB) and ultraviolet C (UVC) light-emitting diodes (LEDs) with focus on the work done previously. Furthermore, approaches to improve the properties of such AlN/sapphire templates by the combination of high-temperature annealing (HTA) and patterned AlN/sapphire interfaces are discussed. While the beneficial effect of HTA is demonstrated for UVC LEDs, the growth of relaxed AlGaN buffer layers on HTA AlN is a challenge. To achieve relaxed AlGaN with a low dislocation density, the applicability of HTA for AlGaN is investigated.

1. Introduction

In recent years ultraviolet (UV) light-emitting diodes (LEDs) entered several fields of applications, e.g., phototherapy, water disinfection, biochemical agent detection, and gas sensing.[1–7] These Al(In)GaN-based LEDs are not only environmental friendly replacements for mercury lamps but also open up new applications due to their compactness, narrow line width, and rapid turn-on/turn-off behavior. For some applications in the UVB (320–280 nm) and UVC (280–200 nm) spectral range, e.g., medical treatment, water purification, and nonline-of-sight communication, UV LEDs with high powers and high efficiencies are needed.[8–10] Unfortunately, in this wavelength range, the devices still suffer from obstacles like limited UV transparency of native AlN bulk substrates or high densities of threading dislocations (TDs) in layers grown on foreign substrates. These TDs lead to nonradiative recombination in the active region.[11,12] Especially for shorter-emission wavelength with increasing Al content in the AlGaN layers challenges are the poor p-type conductivity, decreasing charge carrier confinement with increasing Al content in the active region, and an increasing amount of TM-polarized light, making light extraction more difficult.[7,13–15]

In this article, we will focus on the improvement of the efficiency of such LEDs by improving the properties of the templates on which they are grown. As bulk AlN with sufficient UV transparency is not readily available, a pseudosubstrate is commonly used, which consists of AlN and AlGaN layers grown on sapphire substrates by vapor phase epitaxy (**Figure 1**). Such pseudosubstrates have to fulfil four key requirements. 1) A low threading dislocation density (TDD) preferably below $10^9 \, \text{cm}^{-2}$, e.g., to reduce nonradiative recombination in the LED active region;[13] 2) surface morphology suitable for further growth, particularly smooth enough for n-AlGaN and quantum well (QW) growth with a well-defined and homogeneous composition; 3) transparency for the emitted UV light, as due to large p-metal contacts and, in case of UVC LEDs also due to nontransparent p-AlGaN, the LEDs are usually fabricated as bottom emitters (i.e., emission through the pseudosubstrate, as shown in Figure 1); and 4) offering a defined in-plane lattice constant which allows for the pseudomorphic growth of the QW region without the onset of relaxation processes (e.g., roughening or dislocation formation).

In the first part of this article, we provide an overview on template technologies including the approaches which we have explored in detail in our group. In the second part, we provide insights into our current routes for further template improvement. Even if semi- and nonpolar AlGaN could have advantages by reducing or avoiding piezoelectric fields and in promoting light extraction of the TM-polarized deep UVC light, this work focuses on the commonly used *c*-plane Al(Ga)N grown by metal–organic vapor phase epitaxy (MOVPE) on *c*-plane-oriented sapphire substrates.

Dr. S. Hagedorn, S. Walde, Dr. A. Knauer, D. Pacak, Dr. C. Netzel, Dr. A. Mogilatenko, Prof. M. Kneissl, Prof. M. Weyers
Ferdinand-Braun-Institut, Leibniz-Institut fuer Hoechstfrequenztechnik
Gustav-Kirchhoff-Str. 4, 12489 Berlin, Germany
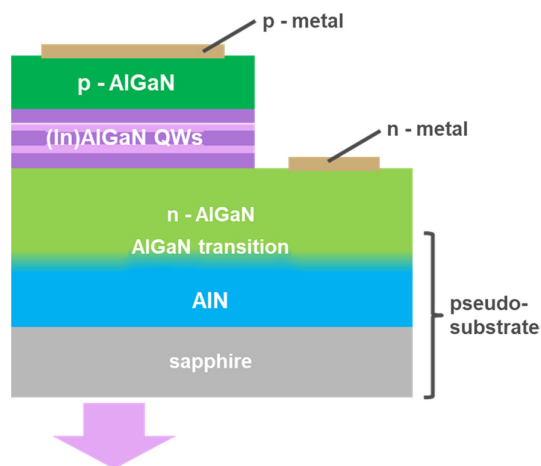E-mail: Markus.Weyers@fbh-berlin.de

N. Susilo, D. Pacak, Dr. T. Wernicke, Prof. M. Kneissl
Institute of Solid State Physics
Technical University Berlin
Hardenbergstr. 36, 10623 Berlin, Germany

L. Cancellara, Dr. C. Hartmann
Leibniz Institute for Crystal Growth
Max-Born-Str. 2, 12489 Berlin, Germany

The ORCID identification number(s) for the author(s) of this article can be found under https://doi.org/10.1002/pssa.201901022.

**Figure 1.** Simplified cross section of a bottom emitter UV LED.

Sylvia Hagedorn received her diploma in physics 2007 from the Technische Universität Berlin. From 2008 to 2015, she worked at Ferdinand-Braun-Institut, Leibniz-Institut fuer Hoechstfrequenztechnik (FBH), Berlin, on AlGaN crystal growth by hydride vapor phase epitaxy. After receiving her PhD in 2015 from TU Berlin, she continued at FBH as a research scientist, working on AlN growth for UV LEDs. Here, she is part of the Joint Lab GaN Optoelectronics between TU Berlin and FBH and involved in the activities to develop UVB and UVC LEDs.

Markus Weyers received his diploma in physics 1986 and his Dr. rer. nat. degree in 1990 from RWTH Aachen, Germany. From 1990 to 1992, he was with NTT Basic Research Labs in Musashino, Japan. Since 1992, he has been head of the Materials Technology Department at Ferdinand-Braun-Institut, Leibniz-Institut fuer Hoechstfrequenztechnik in Berlin, Germany. He also is adjunct professor at TU Berlin. His research interests include MOVPE growth of GaAs- and GaN-based laser structures and UV LEDs and GaN transistor structures.

2. AlN on Sapphire—Strain Management and TDD Reduction

The lattice mismatch between AlN and sapphire usually leads to an island-like growth start. Ideally, misfit dislocations, which propagate in plane, are formed to overcome the lattice mismatch. But as the AlN nuclei can be tilted and twisted toward each other, TDs with out-of-plane components are built during coalescence of the islands. These TDs spread in growth direction and can thus negatively influence the subsequently grown LED heterostructure. Typical TDDs for the first 100 nm AlN grown on sapphire are in the range of 10^{11}–10^{12} cm^{-2} and hence at least two orders of magnitude too high for serving as a reasonable base for UV LEDs. Therefore, in recent years, several techniques to decrease the dislocation density were developed.

2.1. Planar AlN Growth

To reach for low TDD, the effect of mutual dislocation annihilation with increasing AlN layer thickness can be exploited. The thicker the AlN layer, the higher the chance that climbing dislocations with opposite Burgers vectors meet each other and annihilate. This requires layer thicknesses of a few micrometers. Therefore, the tensile stress, which can lead to cracking after growth of only a few hundred nanometers of continuous, smooth AlN, must be reduced. Special attention has therefore to be paid to the growth start on sapphire, comprising the preconditioning of the MOVPE reactor. Several approaches to manage the tensile strain take advantage of a mixed polarity AlN growth start where N-polar domains can be laterally overgrown by Al-polar domains. It has been shown that the ratio of N-polar and Al-polar areas can be controlled during growth start by controlling oxygen and/or humidity in the MOVPE reactor.[16–20] Another way to control the N-polar to Al-polar ratio is by NH$_3$ preflow (nitridation) or TMAl preflow over the sapphire surface during heating till AlN growth temperature.[21,22] Other approaches to increase the AlN layer thickness introduce "rough-to-smooth" growth steps, i.e., 3D to 2D growth, to achieve strain management, e.g., by the ammonia pulse-flow method or by varying the V/III ratio.[23,24] By this, crack-free, smooth layers of 3–4 μm thickness can be obtained. Another approach to manage the tensile strain is the self-organized void formation at the AlN/sapphire interface by annealing a 100 nm-thick AlN starting layer at a relatively high temperature of 1450 °C in H$_2$—N$_2$—NH$_3$ atmosphere.[25] This technique enables thick AlN layer growth without cracking. However, most commercial MOVPE machines cannot reach the required high temperatures.

In our lab, we realize growth of crack-free AlN in a production scale 11 × 2 in.^{2} MOVPE reactor by a "rough-to-smooth" growth approach.[26] Therefore, the initial roughening is determined by managing the N-polar to Al-polar AlN transition at the growth start (**Figure 2**). The rough layer is grown using a high V/III ratio for the first 500 nm before coalescence is achieved by decreasing the V/III ratio. By this approach, AlN layers of up to 2 μm thickness with a TDD of 4×10^9 cm^{-2} can be grown without cracking, indicated as "planar growth" in **Figure 3**. Higher layer thicknesses up to 3.5 μm can be reached by roughening the sapphire surface in H$_2$ atmosphere at 1290 °C prior to AlN growth. Thereby a further decrease in the TDD down to 2×10^9 cm^{-2} (Figure 3) is realized.[27] However, to reproducibly reach TDDs of 10^9 cm^{-2} across a whole wafer is challenging and with increasing AlN layer thickness also the residual wafer bow after cooling down increases, leading to problems in the UV LED chip process like vacuum chuck handling or a curved focus plane in lithography.
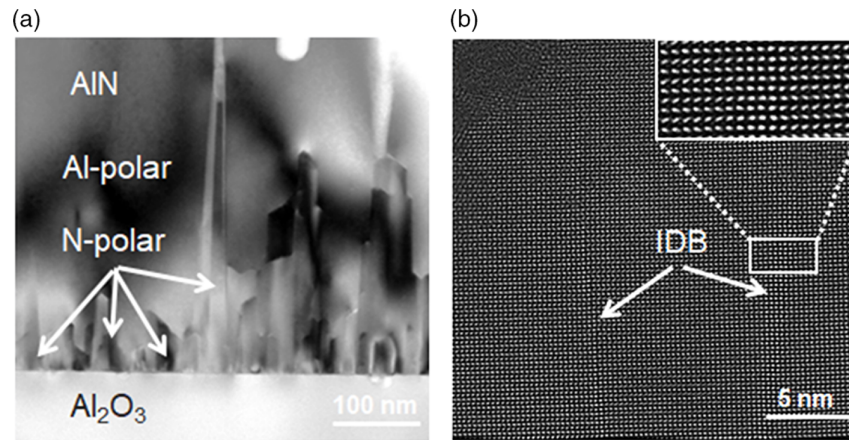
Figure 2. a) Cross-section bright-field TEM image with $g = [0002]$ indicating mixed AlN polarity at the AlN/sapphire interface and b) high-resolution transmission electron microscopy (HRTEM) image in the [11-20] zone axis of the same sample, showing inversion domain boundaries (IDB) between areas of different polarities.
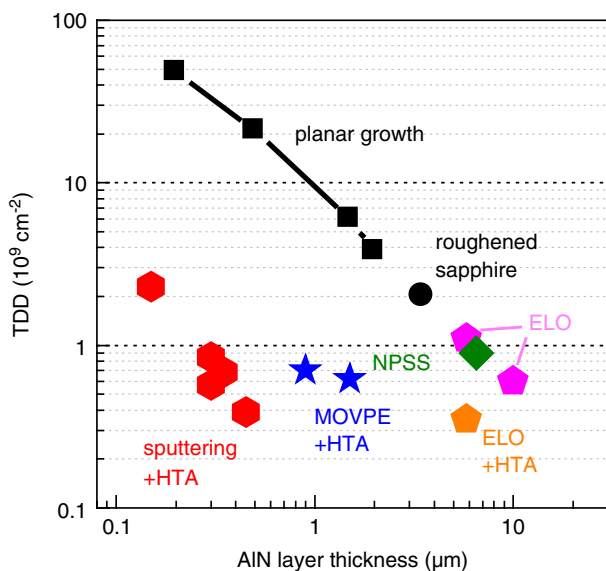
Figure 3. TDD over AlN layer thickness reached for different TDD reduction techniques investigated by our group.

2.2. High-Temperature Annealing for TDD Reduction

In 2016, a new approach to decrease the TDD down to about $5 \times 10^8 \, \text{cm}^{-2}$ even for thin AlN layers with thickness below $1 \, \mu\text{m}$ was published by Miyake et al.[28] High-temperature annealing (HTA) at about $1700 \, ^\circ\text{C}$ in N_2–CO atmosphere was applied for MOVPE-grown layers, leading to a rearrangement of the AlN crystal lattice, reducing the TDD by more than one order of magnitude. This promising approach can also be applied to sputtered AlN, which can help to avoid the sensitive nucleation process in MOVPE reactors.[29] Face-to-face arrangement of the AlN/sapphire templates during HTA was found to preserve the AlN surfaces from decomposition.[29] Hence, the toxic N_2—CO ambient during annealing can be avoided. The HTA technique has greatly influenced the AlN/sapphire community in recent years. Even the first UVC LEDs have been successfully fabricated on HTA templates.[30] By adjusting the sputtering process, TDDs of down to $2 \times 10^8 \, \text{cm}^{-2}$ for AlN on sapphire were achieved.[31] Further analysis was conducted to gain a deeper understanding of the impact of HTA on the AlN material quality, e.g., domain boundary movement, strain development, and dislocation movement mechanisms via dislocation climbing.[32–35]

Our group investigated the annealing of sputtered AlN regarding the impact of HTA conditions on the MOVPE growth of AlN on such HTA templates.[36] Low TDDs of down to $4 \times 10^8 \, \text{cm}^{-2}$ were reached after annealing, labeled "sputtering + HTA" in Figure 3, but for some samples problems in further MOVPE growth occurred. Especially for thin sputtered layers and high annealing temperatures, columnar AlN growth was observed. We have found a partial blocking of the surface of sputtered AlN layers after the HTA process by epitaxial AlON as the cause. Cross-sectional transmission electron microscopy (TEM) measurements (**Figure 4**) of MOVPE AlN grown on a 350 nm-thick, sputtered AlN layer annealed at high temperatures show the disturbance of the homoepitaxial interface by AlON islands. Hence, thick sputtered layers should be favored when high temperatures are applied during HTA. For example, 450 nm-sputtered AlN annealed at $1700 \, ^\circ\text{C}$ was successfully overgrown with AlN with an atomically smooth surface by MOVPE, whereas on 350 nm-thick AlN annealed at $1700 \, ^\circ\text{C}$, extended AlON formation on the surface occurred.[36]

Further works of our group focused on the HTA of MOVPE-grown AlN layers. We investigated the influence of an intermediate HTA step on the growth of $1.6 \, \mu\text{m}$ AlN on sapphire.[26] The TDD could be decreased by an order of magnitude down to $6 \times 10^8 \, \text{cm}^{-2}$ (labelled as "MOVPE + HTA" in Figure 3) while maintaining an atomically smooth surface.

In conclusion, HTA is a versatile technique to reduce the dislocation density and the required AlN layer thickness at the same time. Still, there are challenges. The surface after HTA has to be smoothened, and the smaller in-plane lattice constant after HTA has to be taken into consideration for further heterostructure growth.[37,29]
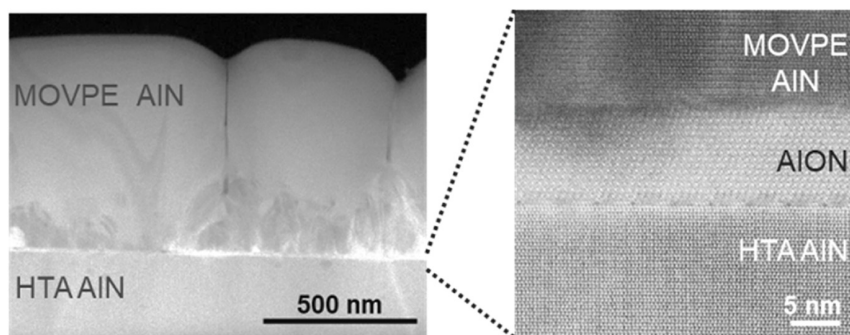
Figure 4. Cross-sectional high-angle annular dark-field–scanning transmission electron microscopy (STEM) image of MOVPE AlN grown on sputtered and high-temperature-annealed AlN taken in the [11-20] zone axis. A higher magnification of the HTA AlN/MOVPE AlN interface (right) shows MOVPE-grown AlN on epitaxially arranged (111) AlON.

2.3. Patterned AlN/Sapphire Interfaces

The technique of epitaxial lateral overgrowth (ELO) to reduce the dislocation density has already been mentioned in Section 2.1, where self-assembled lateral growth was introduced by "rough-to-smooth" growth approaches. In the laterally overgrown regions, the dislocations can bend toward open surfaces by image forces, preventing them from spreading in growth direction, and strain can be released. The lateral growth can be provoked by an intentional patterning of an AlN/sapphire substrate, as published by Hirayama et al.[38] Hirayama et al. showed that the regions which were laterally grown over the trenches offer a lower TDD of $3 \times 10^8 \, cm^{-2}$ compared with the AlN regions grown above the ridges where the TDD of $2 \times 10^9 \, cm^{-2}$ was still about an order of magnitude higher.

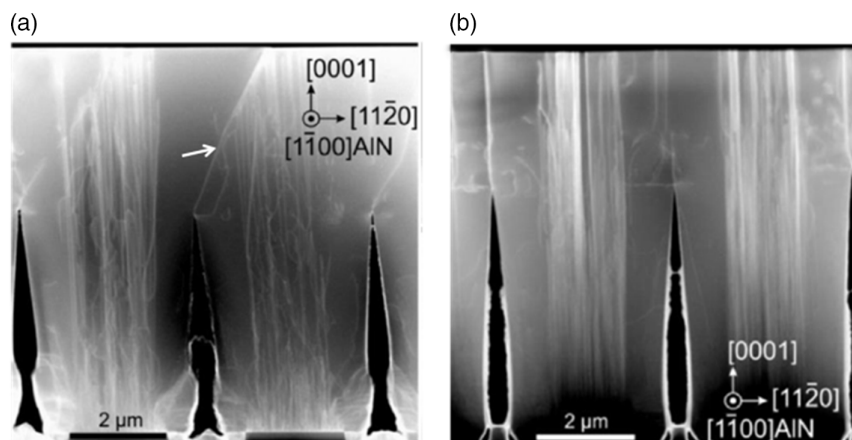Our group investigated in detail the overgrowth of patterned AlN/sapphire substrates with a pitch of 3.5 μm fabricated by photolithography and dry etching (**Figure 5**). The influence of the pattern orientation, the substrate off-cut direction, and off-cut angle on the ELO growth were examined. We found that for smooth overgrowth and to promote coalescence a-plane-oriented AlN trench sidewalls and a sapphire off-cut angle perpendicular to the stripes are beneficial, i.e., AlN stripes running along the [11-20] sapphire direction.[39] A sapphire off-cut angle of 0.2° perpendicular to the trench direction leads
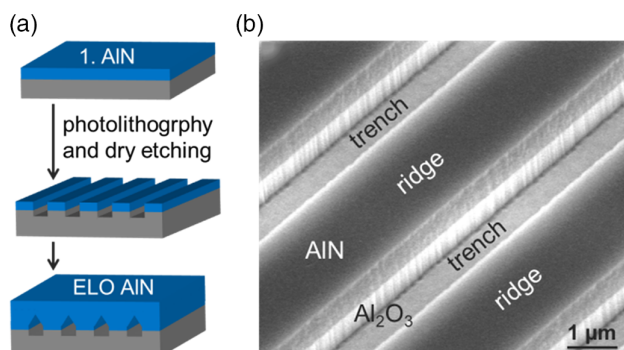
to the build up of 15 nm-high macrosteps during coalescence for geometrical reasons. During coalescence a 2D inclined grain boundary is formed which collects many dislocations even above the ridges during further growth (**Figure 6**a). Unfortunately, the macrosteps remain on the surface, causing inhomogeneities in AlGaN composition during subsequent device growth.[40–42] To avoid macrosteps on the surface, a reduction of the off-cut angle down to 0.1° perpendicular to the trench direction was applied. By this, the advantage of the grain boundary-collecting dislocations gets lost (Figure 6b), and the TD distribution is stripe like with low $10^8 \, cm^{-2}$ in the laterally grown areas and low $10^9 \, cm^{-2}$ over ridges and along the coalescence lines, resulting in an average TDD of $1.1 \times 10^9 \, cm^{-2}$ for 6 μm-thick AlN layers, as shown in Figure 3 as "ELO."[43,30] Such ELO templates have been successfully used by our collaboration partners at the Technical University Berlin for UVC LED growth.[30,6]

Actually, avoiding the two-step epitaxy for ELO (Figure 5a) by directly patterning the sapphire substrate would save costs. This approach is more challenging because the lateral growth is hindered by misaligned growth from non-c-plane sapphire facets, e.g., the sidewalls of the trenches.[44] However, due to the low TDD reached by the HTA technique, as described in Section 2.2, costly lithography and dry etching steps to intentionally pattern AlN/sapphire or sapphire seem no longer necessary to decrease the TDD. But if designed in the right way, the patterned interface does not only help decrease the TDD and the strain by lateral overgrowth but also improves the light outcoupling from the AlN/sapphire substrate by partially avoiding the total internal reflection at the AlN/sapphire interface. For UVC LEDs grown on ELO AlN with 3.5 μm pitch stripe patterns at the interface (Figure 6b), calculations and experiments reveal an improvement of the LEE of about 13% compared with a planar AlN/sapphire interface as light under a high incidence angle is refracted at the voids.[30] In this context, AlN grown on nanoscale patterned sapphire substrates (NPSSs) comes into focus. Such nanosize patterns not only decrease the coalescence layer thickness compared with microsize patterns, as described in the previous section, but if arranged in a periodical way, they are also supposed to have a photonic crystal effect, potentially avoiding parts of the internal total reflection.[45–48] Although GaN growth on microsize patterned sapphire substrates (PSS) is a state-of-the-art technology for blue LEDs, reports on UV

Figure 5. a) A schematic representation of the process for the production of AlN ELO substrates. b) SEM image of a stripe-patterned AlN/sapphire substrate with 3.5 μm pitch.

Figure 6. Cross-sectional annular dark field–STEM image of ELO AlN on trench-patterned AlN/sapphire with a) 0.2° and b) 0.1° sapphire off-cut perpendicular to the ridge. Reproduced with permission.[43] Copyright 2016, Wiley-VCH.

LEDs on NPSS are limited.[49] This concept is still under investigation for UVB and UVC LEDs. Wave optical simulations are needed to describe the interaction of light with an AlN/NPSS interface. Such simulations suggest an increase in AlN/sapphire transmissivity for AlN/NPSS interfaces for highly transparent and reflective p-sides.[50]

Mainly due to the high sticking coefficient of Al, MOVPE growth of AlN on NPSS is challenging. Growth conditions have to be properly adjusted to suppress polycrystalline growth in the presence of non-*c*-plane-oriented sapphire facets.[51,52] We reached the overgrowth of pillar-like NPSS with a pitch of 1 μm and avoided surface steps by decreasing the off-cut angle from 0.2° to 0.1°.[51,53] TDDs of 9×10^8 cm^{-2} for 7 μm-thick AlN on pillar-like NPSS (**Figure 7**a) have been demonstrated by etch pit density (EPD, Figure 7b) and electron channeling contrast imaging, shown in Figure 3 as "NPSS."[53] However, the coalescence layer thickness for growth on pillar-like NPSS is relatively high and new dislocations are introduced when the AlN islands growing on adjacent pillars coalesce.[51] Therefore, a hole-like pattern which provides a continuous sapphire surface around the holes and hence with a continuous AlN layer (instead of isolated islands for the pillar-like structures) from the growth start appears to be more practical in keeping the coalescence

thickness low and in avoiding dislocation introduction during coalescence.

Our group also recently investigated the usage of HTA to avoid tensile strain and lower the TDD for MOVPE AlN on hole-type NPSS with a pitch of 600 nm.[54] By introducing HTA at 1680 °C for 1 h after the growth of 300 nm AlN, cracking during further overgrowth of the NPSS could be prevented, and fully coalesced AlN was realized at a total AlN layer thickness of only 800 nm.

2.4. Combination of ELO and HTA

As the outcome of our studies of UVC LEDs grown on different templates was that the combination of HTA (for low TDD) and a patterned AlN/sapphire interface (for enhanced light extraction) increases the light output power of LEDs, an investigation of the combination of both approaches was the natural next step.[30] We found that in terms of reproducibility and low defect density, the adaption of the ELO process (Figure 5a) by introducing an intermediate HTA step after deposition of a 300 nm-thick AlN cover layer on the patterned template works best (**Figure 8**a). By this, we were able to achieve an atomically smooth surface (Figure 8b) and decrease the TDD from 1×10^9

EPD = 9×10^8 cm^{-2}
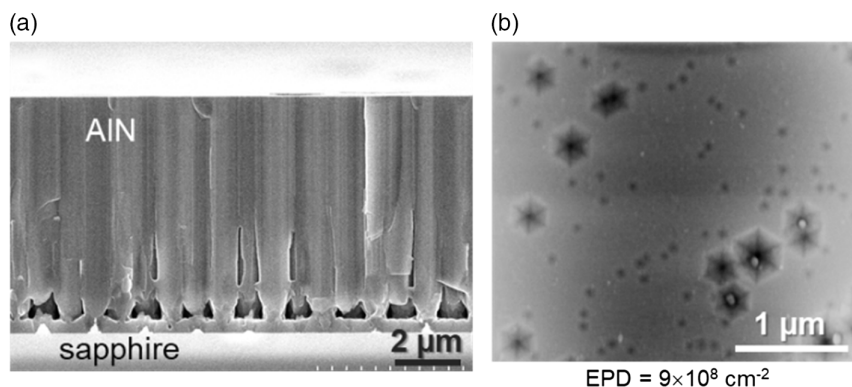
Figure 7. a) Cross-sectional SEM image of 7 μm-thick AlN grown on pillar-type NPSS and b) SEM image of KOH etch pits on the sample surface.
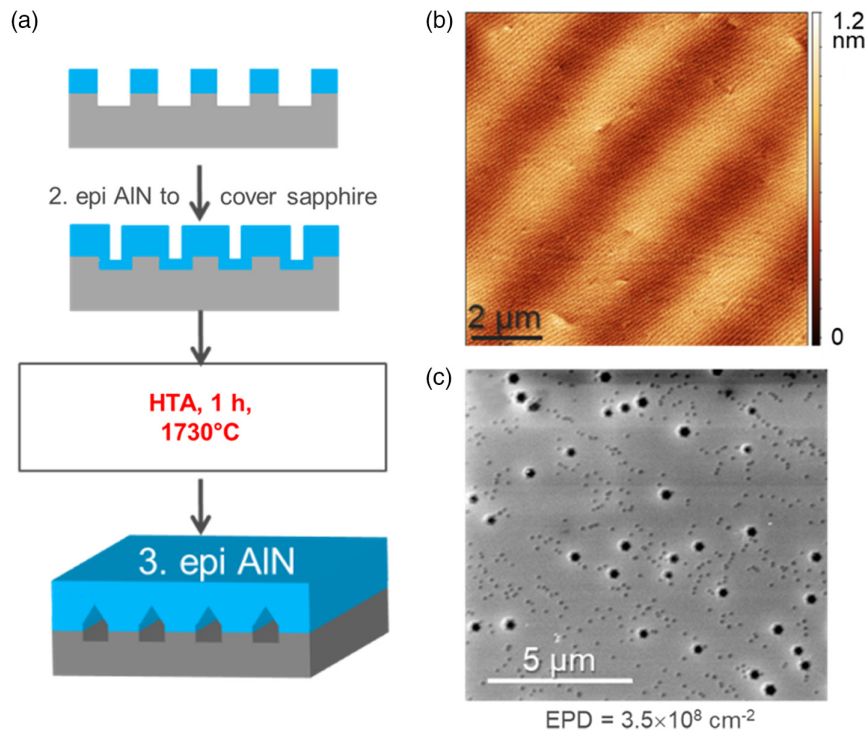
Figure 8. a) Sketch of the process scheme to combine HTA and ELO with protection of the patterned interface by 300 nm-AlN cover layer prior to HTA. b) AFM topogram of 6 μm ELO AlN and c) corresponding surface EPD determined from surface SEM image.

to $3.5 \times 10^8 \, cm^{-2}$, as verified by the EPD on the sample surface (Figure 8c), labeled as "ELO + HTA" in Figure 3.

An ELO AlN/sapphire template, as shown in Figure 6b, and an HTA ELO AlN/sapphire template were simultaneously overgrown with a 265 nm LED heterostructure to test the usability of HTA ELO AlN for UVC LEDs. The corresponding LED chip light-current-voltage (LIV) characteristics for both samples in **Figure 9** show a higher output power of LEDs with HTA ELO AlN. Hence for a high light output power, the combination of ELO and HTA is a promising approach.[55]

3. Current Approaches to Improve Templates for UVB LEDs

3.1. AlGaN for UVB LEDs

UVC LED heterostructures can be grown pseudomorphically on AlN native substrates as well as on AlN/sapphire templates with a very low TDD obtained by, for example, combining HTA with NPSS. AlGaN-based UVB LEDs with Al mole fractions of 0.6 or lower are more challenging as strain relaxation during AlGaN growth has to be mastered. The relaxation usually takes place by a roughening of the AlGaN surface and formation of misfit dislocation segments.[56,57] As with AlN, approaches such as introducing superlattices, rough-to-smooth growth, and overgrowth of patterned substrates were applied to manage the compressive strain and decrease the TDD.[24,56,58–61] For the rough-to-smooth growth techniques as well as for ELO on
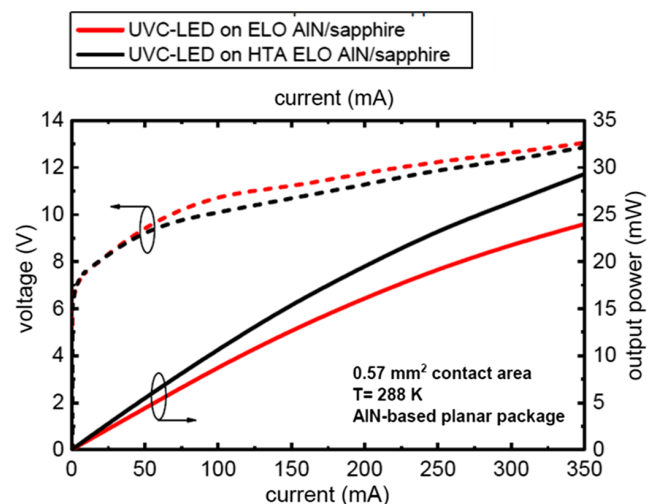
Figure 9. LIV characteristics (integrated sphere measurement) of mounted 265 nm UVC LED chips showing a higher output power for HTA ELO AlN compared with ELO AlN without HTA.

patterned substrates, the obstacle of composition inhomogeneities due to different surface diffusion lengths of Ga and Al has to be overcome.[59–63]

Figure 10 shows the in situ curvature and reflectance (at 405 nm) transients of AlGaN growth for UVB LEDs, starting with an AlN/GaN superlattice (resulting in average
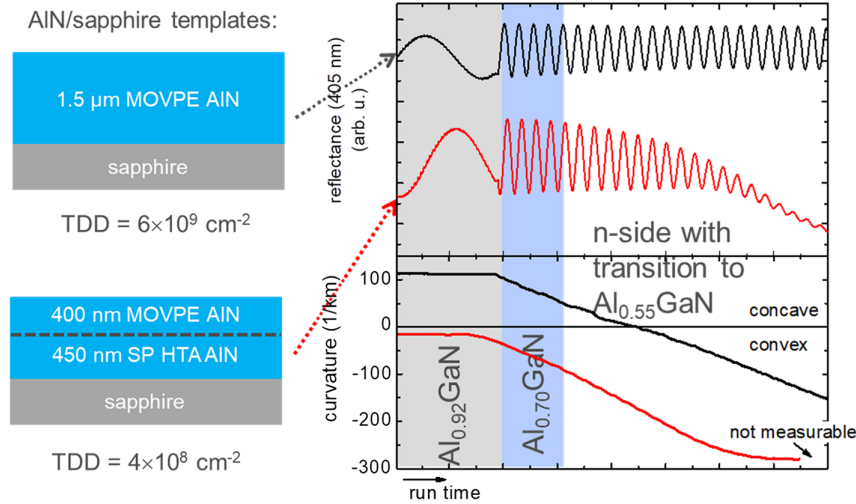
Figure 10. In situ measurement of 405 nm reflection from the sample surface and corresponding wafer curvature during AlGaN transition layer growth for UV LEDs on two different kinds of AlN/sapphire templates. For heavily roughened AlGaN, the curvature signal measurement by laser reflection is not possible (arrow).

$Al_{0.92}Ga_{0.08}N$), followed by transition to n-$Al_{0.55}Ga_{0.45}N$ as reported in a previous study.[64] The AlGaN was deposited simultaneously on an MOVPE-grown AlN/sapphire template with 1.5 μm AlN layer thickness (TDD $= 6 \times 10^9$ cm^{-2}) and on a sputtered AlN template treated by HTA (TDD $= 4 \times 10^8$ cm^{-2}). The decreasing reflectance from the HTA-based wafer indicates roughening of the AlGaN surface, whereas on the simultaneously overgrown template without annealing, the surface stays smooth. The curvature transients show that the AlGaN grows under compressive strain. For the HTA-based template, a sudden strain relaxation occurs, indicated by the change in the slope of the curvature transient to the horizontal in conjunction with the onset of surface roughening. We assume that the onset of strain relaxation on the
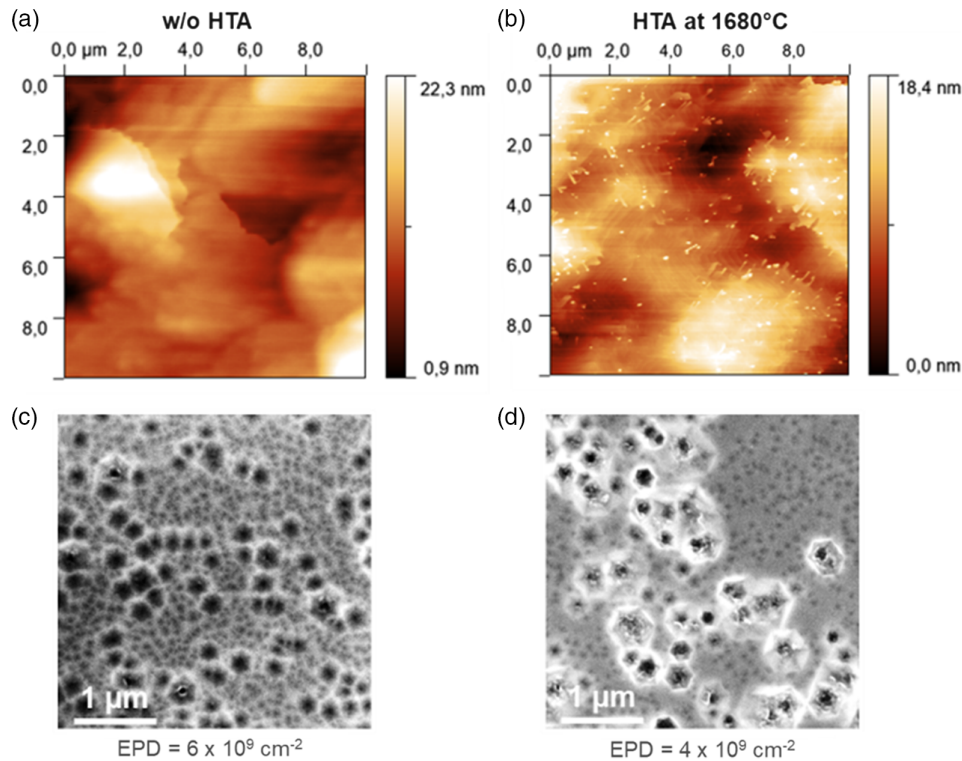
Figure 11. AFM surface topograms of 2 μm-thick $Al_{0.75}Ga_{0.25}N$ a) before and b) after HTA at 1680 °C for 1 h and corresponding SEM images of EPD for the sample c) without and d) with HTA.
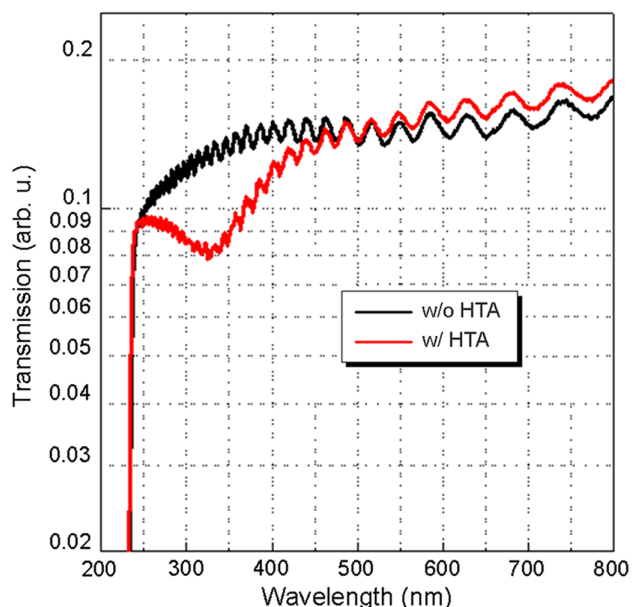
Figure 12. Transmission spectra of 1.3 µm $Al_{0.75}Ga_{0.25}N$ before and after HTA at 1680 °C for 1 h.

HTA template is on the one hand caused by the lower TDD, hence, less TDs can incline from the vertical direction to lower the compressive strain, and on the other hand, by the lower in-plane lattice constant inherent to HTA AlN layers.[29,37] This experiment opens up the question of how necessary it is to offer a low TDD AlN/template as the base layer for UVB LEDs. However, to use HTA AlN for UVB LEDs, AlGaN transition layer growth processes have to be adapted to the low TDD and lower in-plane lattice constant compared with MOVPE-grown AlN base layers, e.g., by changing growth parameters to smoothen the AlGaN after roughening.[56,65]

3.2. HTA of AlGaN

As shown in the previous section, the growth of AlGaN base layers for UVB LEDs is challenging due to the necessity to manage the strain relaxation processes introduced by the lattice mismatch between AlN and AlGaN. Actually, to realize the pseudomorphic growth of UVB LEDs, it would be convenient to grow on AlGaN bulk substrates. These unfortunately do not exist and thus, comparable with the situation with UVC LEDs on AlN, ways to lower the TDD in AlGaN are also required. Therefore, we are investigating the impact of HTA on AlGaN. About 1.3 µm-thick $Al_{0.75}Ga_{0.25}N$ layers were grown on 630 nm-thick AlN on sapphire and annealed at 1680 °C for 1 h. Atomic force microscopy (AFM) surface topograms (**Figure 11**a,b) show that the overall roughness of the AlGaN surface does not change. Due to HTA, some small steps of 0.5 nm height and small islands of about 100 nm in diameter are formed on the surface. Determining the EPD for the annealed and nonannealed samples (Figure 11c,d) reveals a TDD reduction from 6×10^9 to 4×10^9 cm^{-2} by HTA. From the position of the band edge in transmission measurements (**Figure 12**) and from X-ray diffraction (XRD) reciprocal space maps (RSM) of the 11–24 reflection (**Figure 13**), it can be concluded that the bulk Al mole fraction does not significantly change. The decrease in the broadening of the reciprocal lattice points for both AlN and AlGaN due to annealing also shows the improvement in crystal quality. Furthermore, both peaks shift toward smaller absolute Q_x values, indicating a decrease in the in-plane lattice constants, whereas the relaxation of the AlGaN layer in relation to AlN slightly decreases from 75% to 70% due to HTA. After HTA, absorption around 325 nm occurs (Figure 12), pointing to defect formation in AlGaN during annealing. The RSM (Figure 13) after annealing shows an increased count rate between the AlN and AlGaN peaks, which suggests the formation of small regions with decreased Ga mole fraction. To further investigate the samples cathodoluminescence (CL) spectra were measured along the cross section of
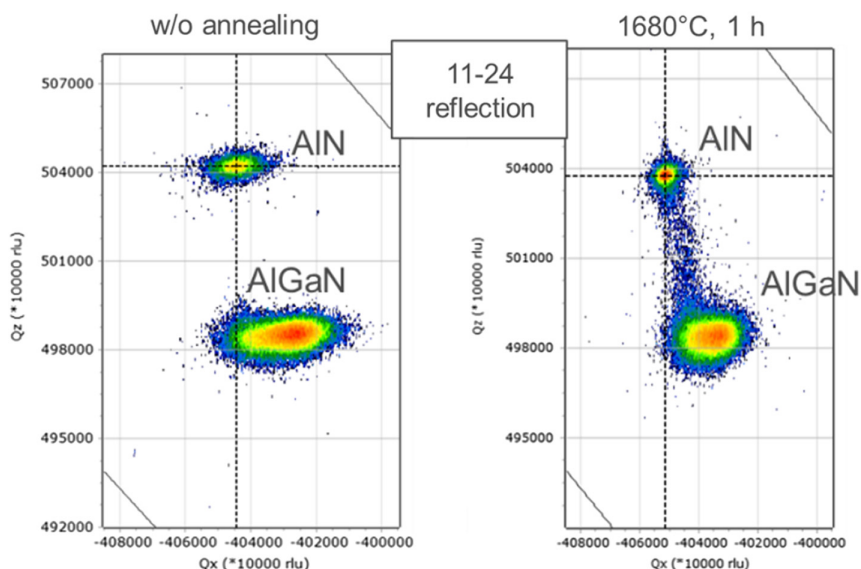
Figure 13. XRD RSM of the asymmetric [11–24] AlN and AlGaN reflections before and after HTA.
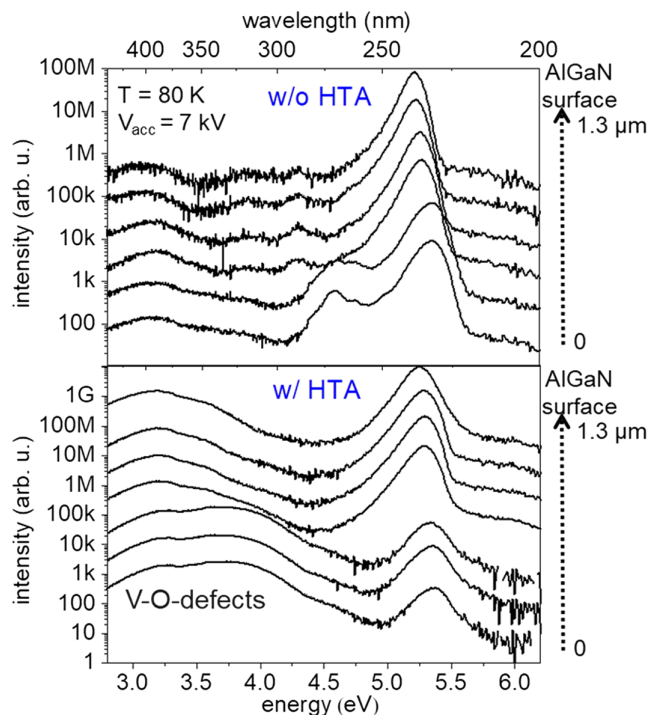
Figure 14. CL measurements of 1.3 μm $Al_{0.75}Ga_{0.25}N$ a) without and b) with annealing at 1680 °C for 1 h taken along the cross section in equidistant steps at 80 K with an acceleration voltage of 7 kV.

AlGaN before and after annealing (**Figure 14**). The band edge-related luminescence wavelength before and after annealing is not significantly different but the defect luminescence in the long wavelength range is increased by HTA. This luminescence can be assigned to complexes involving metal vacancies and oxygen.[66–68] However, there is no clear assignment of a specific complex to a particular peak. It is interesting to note that the spectral shape changes with depth after HTA (and also without HTA but to a much lesser extent). Close to the AlN interface after HTA the peak around 3.8 eV is dominant, whereas toward the surface, the one around 3.2 eV is stronger. The reason for this is unclear, and we can only speculate that in the depth O coming from the sapphire substrate and through the AlN buffer during HTA is gettered (presumably at the misfit dislocations formed here), whereas the loss of Ga (in other words: formation of Ga vacancies) dominates close to the surface. Such a point defect formation could also be the cause for the absorption around 325 nm (Figure 12). Most probably, the vacancy formation is triggered by the low Ga—N binding energy compared with Al—N. To successfully anneal AlGaN, high Al mole fractions and lower annealing temperatures than for HTA of AlN appear reasonable.

4. Conclusions

In this work, we provided an overview on the current status of AlN/sapphire templates for UVB and UVC LEDs with a focus on the work done by our group. Substrates for UVC LEDs with a low

TDD, smooth surfaces, and AlN/sapphire interfaces promoting light extraction can be provided by combining HTA and patterned substrates such as NPSS. The template technology for UVB LEDs still has to be developed further. As in this case it is not possible to pseudomorphically grow on AlN, ways are needed to relieve the strain in the AlGaN buffer layer without generating point defects that give rise to absorption or a high TDD. We have shown a possible way to reduce the TDD of AlGaN by annealing the samples at temperatures of 1680 °C, but to benefit from this process, the formation of UV-absorbing lattice defects must be suppressed.

Conflict of Interest

The authors declare no conflict of interest.

[1] W. L. Morison, T. B. Fitzpatrick, *Phototherapy and Photochemotherapy of Skin Disease*, Raven Press, New York **1991**.
[2] M. Kneissl, J. Rass, *Springer Series in Materials Science*, Springer, Berlin/New York **2016**.
[3] M. Würtele, T. Kolbe, M. Lipsz, A. Külberg, M. Weyers, M. Kneissl, M. Jekel, *Water Res.* **2011**, *45*, 1481.
[4] H. Hirayama, T. Yatabe, N. Noguchi, N. Kamata, *Electron. Commun. Jpn.* **2010**, *93*, 24.
[5] M. Martens, F. Mehnke, C. Kuhn, C. Reich, V. Kueller, A. Knauer, C. Netzel, C. Hartmann, J. Wollweber, J. Rass, T. Wernicke, M. Bickermann, M. Weyers, M. Kneissl, *IEEE Photonics Technol. Lett.* **2014**, *26*, 342.
[6] F. Mehnke, M. Guttmann, J. Enslin, C. Kuhn, C. Reich, J. Jordan, S. Kapanke, A. Knauer, M. Lapeyrade, U. Zeimer, H. Krüger, M. Rabe, S. Einfeldt, T. Wernicke, H. Ewald, M. Weyers, M. Kneissl, *IEEE J. Sel. Top. Quantum Electron.* **2017**, *23*, 2000108.
[7] A. Khan, K. Balakrishnan, T. Katona, *Nat. Photonics* **2008**, *2*, 77.
[8] M. Schreiner, J. Martínez-Abaigar, J. Glaab, M. Jansen, *Optik Photonik* **2014**, *9*, 34.
[9] S. Vilhunen, H. Särkkä, M. Sillanpää, *Environ. Sci. Pollut. Res.* **2009**, *16*, 439.
[10] M. H. Crawford, M. A. Banas, M.-P. Ross, D. S. Ruby, J. S. Nelson, R. Boucher, A. A. Allerman, *Final LDRD Report: Ultraviolet Water*

Purification Systems for Rural Environments and Mobile Applications, SAND2005-7245, Sandia National Laboratories **2005**.

[11] S. Y. Karpov, Y. N. Makarov, *Appl. Phys. Lett.* **2002**, *81*, 4721.

[12] M. Kneissl, T.-Y. Seong, J. Han, H. Amano, *Nat. Photonics* **2019**, *13*, 233.

[13] M. Kneissl, T. Kolbe, C. Chua, V. Kueller, N. Lobo, J. Stellmach, A. Knauer, H. Rodriguez, S. Einfeldt, Z. Yang, N. M. Johnson, M. Weyers, *Semicond. Sci. Technol.* **2011**, *26*, 014036.

[14] P. Pampili, P. J. Parbrook, *Mater. Sci. Semicond. Process.* **2017**, *62*, 180.

[15] Y.-H. Liang, E. Towe, *Appl. Phys. Rev.* **2018**, *5*, 011107.

[16] B. Kuhn, F. Scholz, *Phys. Status Solidi A* **2001**, *188*, 629.

[17] J. Bläsing, A. Krost, J. Hertkorn, F. Scholz, L. Kirste, A. Chuvilin, U. Kaiser, *J. Appl. Phys.* **2009**, *105*, 033504.

[18] S. Mohn, N. Stolyarchuk, T. Markurt, R. Kirste, M. P. Hoffmann, R. Collazo, A. Courville, R. Di Felice, Z. Sitar, P. Vennegues, M. Albrecht, *Phys. Rev. Appl.* **2016**, *5*, 054004.

[19] D. D. Koleske, J. J. Figiel, D. L. Alliman, B. P. Gunning, J. M. Kempisty, J. R. Creighton, A. Mishima, K. Ikenaga, *Appl. Phys. Lett.* **2017**, *110*, 232102.

[20] N. Stolyarchuk, T. Markurt, A. Courville, K. March, J. Zuniga-Perez, P. Vennegues, M. Albrecht, *Sci. Rep.* **2018**, *8*, 14111.

[21] M. Funato, M. Shibaoka, Y. Kawakami, *J. Appl. Phys.* **2017**, *121*, 085304.

[22] H. Sun, F. Wu, Y. J. Park, T. M. Al Tahtamouni, K.-H. Li, N. Alfaraj, T. Detchprohm, R. D. Dupuis, X. Li, *Appl. Phys. Lett.* **2017**, *110*, 192106.

[23] H. Hirayama, T. Yatabe, N. Noguchi, T. Ohashi, N. Kamata, *Appl. Phys. Lett.* **2007**, *91*, 071901.

[24] N. Okada, N. Kato, S. Sato, T. Sumii, T. Nagai, N. Fujimoto, M. Imura, K. Balakrishnan, M. Iwaya, S. Kamiyama, H. Amano, I. Akasaki, H. Maruyama, T. Takagi, T. Noro, A. Bandoh, *J. Crystal Growth* **2007**, *298*, 349.

[25] J. Tajima, Y. Kubota, M. Ishizuki, T. Nagashima, R. Togashi, H. Murakami, Y. Kumagai, K. Takada, A. Koukitu, *Phys. Status Solidi C* **2009**, *6*, S447.

[26] S. Walde, S. Hagedorn, M. Weyers, *Jpn. J. Appl. Phys.* **2019**, *58*, SC1002.

[27] S. Hagedorn, A. Knauer, F. Brunner, A. Mogilatenko, U. Zeimer, M. Weyers, *J. Crystal Growth* **2017**, *479*, 16.

[28] H. Miyake, G. Nishio, S. Suzuki, K. Hiramatsu, H. Fukuyama, J. Kaur, N. Kuwano, *Appl. Phys. Exp.* **2016**, *9*, 025501.

[29] H. Miyake, C.-H. Lin, K. Tokoro, K. Hiramatsu, *J. Crystal Growth* **2016**, *456*, 155.

[30] N. Susilo, S. Hagedorn, D. Jaeger, H. Miyake, U. Zeimer, C. Reich, B. Neuschulz, L. Sulmoni, M. Guttmann, F. Mehnke, C. Kuhn, T. Wernicke, M. Weyers, M. Kneissl, *Appl. Phys. Lett.* **2018**, *112*, 041110.

[31] K. Uesugi, Y. Hayashi, K. Shojiki, H. Miyake, *Appl. Phys. Express* **2019**, *12*, 065501.

[32] J. Kaur, N. Kuwano, K. Jamaludin, M. Mitsuhara, H. Saito, S. Hata, S. Suzuki, H. Miyake, K. Hiramatsu, H. Fu-kuyama, *Appl. Phys. Express* **2016**, *9*, 065502.

[33] S. Xiao, R. Suzuki, H. Miyake, S. Harada, T. Ujihara, *J. Crystal Growth* **2018**, *502*, 41.

[34] L. Cancellara, S. Hagedorn, S. Walde, D. Jaeger, S. Washiyama, I. Gamov, K. Irmscher, T. Markurt, R. Collazo, Z. Sitar, M. Weyers, M. Albrecht, Presented at the Int. Workshop on Nitride Semiconductors, Kanazawa, Japan, (November 2018).

[35] M. X. Wang, F. J. Xu, N. Xie, Y. H. Sun, B. Y. Liu, W. K. Ge, X. N. Kang, Z. X. Qin, X. L. Yang, X. Q. Wang, B. Shen, *Appl. Phys. Lett.* **2019**, *114*, 112105.

[36] S. Hagedorn, S. Walde, A. Mogilatenko, M. Weyers, L. Cancellara, M. Albrecht, D. Jaeger, *J. Crystal Growth* **2019**, *512*, 142.

[37] M. Nemoz, R. Dagher, S. Matta, A. Michon, P. Vennéguès, J. Brault, *J. Crystal Growth* **2017**, *461*, 10.

[38] H. Hirayama, S. Fujikawa, J. Norimatsu, T. Takano, K. Tsubaki, N. Kamata, *Phys. Status Solidi C* **2009**, *6*, S356.

[39] V. Kueller, A. Knauer, U. Zeimer, H. Rodriguez, A. Mogilatenko, M. Kneissl, M. Weyers, *Phys. Status Solidi C* **2011**, *8*, 2022.

[40] U. Zeimer, V. Kueller, A. Knauer, A. Mogilatenko, M. Weyers, G. Tränkle, *J. Crystal Growth* **2013**, *377*, 32.

[41] A. Mogilatenko, V. Kueller, A. Knauer, J. Jeschke, U. Zeimer, M. Weyers, G. Tränkle, *J. Crystal Growth* **2014**, *402*, 222.

[42] A. Mogilatenko, A. Knauer, U. Zeimer, M. Weyers, *Semicond. Sci. Technol.* **2016**, *31*, 025007.

[43] A. Knauer, A. Mogilatenko, S. Hagedorn, J. Enslin, T. Wernicke, M. Kneissl, M. Weyers, *Phys. Status Solidi B* **2016**, *253*, 809.

[44] S. A. Newman, D. S. Kamber, T. J. Baker, Y. Wu, F. Wu, Z. Chen, S. Nakamura, J. S. Speck, S. P. DenBaars, *Appl. Phys. Lett.* **2009**, *94*, 121906.

[45] E. Matioli, C. Weisbuch, *J. Phys. D: Appl. Phys.* **2010**, *43*, 354005.

[46] D. Lee, J. Lee, J. Jang, I.-S. Shin, L. Jin, J. H. Park, J. Kim, J. Lee, H.-S. Noh, Y.-I. Kim, Y. Park, G.-D. Lee, Y. Park, J. Kim, E. Yoon, *Appl. Phys. Lett.* **2017**, *110*, 191103.

[47] H. Hirayama, N. Maeda, S. Fujikawa, S. Toyoda, N. Kamata, *Jpn. J. Appl. Phys.* **2014**, *53*, 100209.

[48] Y. K. Ooi, J. Zhang, *IEEE Photonics J.* **2018**, *10*, 8200913.

[49] P. Dong, J. Yan, J. Wang, Y. Zhang, C. Geng, T. Wei, P. Cong, Y. Zhang, J. Zeng, Y. Tian, L. Sun, Q. Yan, J. Li, S. Fan, Z. Qin, *Appl. Phys. Lett.* **2013**, *102*, 241113.

[50] P. Manley, S. Walde, S. Hagedorn, M. Hammerschmidt, S. Burger, C. Becker, *Opt. Express* **2020**, *28*, 3619.

[51] S. Hagedorn, A. Knauer, A. Mogilatenko, E. Richter, M. Weyers, *Phys. Status Solidi A* **2016**, *213*, 3178.

[52] L. Zhang, F. Xu, J. Wang, C. He, W. Guo, M. Wang, B. Sheng, L. Lu, Z. Qin, X. Wang, Bo Shen, *Sci. Rep.* **2016**, *6*, 35934.

[53] S. Walde, S. Hagedorn, P.-M. Coulon, A. Mogilatenko, C. Netzel, J. Weinrich, N. Susilo, E. Ziffer, L. Matiwe, C. Hartmann, G. Kusch, A. Alasmari, G. Naresh-Kumar, C. Trager-Cowan, T. Wernicke, T. Straubinger, M. Bickermann, R. W. Martin, P. A. Shields, M. Kneissl, M. Weyers, *J. Crystal Growth* **2020**, *531*, 125343.

[54] S. Hagedorn, presented at ICNS, Combining nano-patterned sapphire and high temperature annealing of AlN for UV LEDs, Bellevue, USA (July 2019).

[55] N. Susilo, presented at ICNS, AlGaN-based deep UV LEDs grown on high temperature annealed epitaxially laterally overgrown AlN/sapphire, Bellevue, USA, (July 2019).

[56] Y. Kawase, S. Ikeda, Y. Sakuragi, S. Yasue, S. Iwayama, M. Iwaya, T. Takeuchi, S. Kamiyama, I. Akasaki, H. Miyake, *Jpn. J. Appl. Phys.* **2019**, *58*, SC1052.

[57] Z. Wu, K. Nonaka, Y. Kawai, T. Asai, F. A. Ponce, Ch Chen, M. Iwaya, S. Kamiyama, H. Amano, I. Akasaki, *Appl. Phys. Express* **2010**, *3*, 11003.

[58] T. Matsumoto, M. A. Khan, N. Maeda, S. Fujikawa, N. Kamata, H. Hirayama, *J. Phys. D: Appl. Phys.* **2019**, *52*, 115102.

[59] A. Bell, R. Liu, U. K. Parasuramaan, F. A. Ponce, S. Kamiyama, H. Amano, I. Akasaki, *Appl. Phys. Lett.* **2004**, *85*, 3417.

[60] V. Kueller, A. Knauer, F. Brunner, U. Zeimer, H. Rodriguez, M. Kneissl, M. Weyers, *J. Crystal Growth* **2011**, *315*, 200.

[61] A. A. Allerman, M. H. Crawford, S. R. Lee, B. G. Clark, *J. Crystal Growth* **2014**, *388*, 76.

[62] M. Iwaya, S. Terao, T. Sano, T. Ukai, R. Nakamura, S. Kamiyama, H. Amano, I. Akasaki, *J. Crystal Growth* **2002**, *237*, 951.

[63] D. G. Zhao, D. S. Jiang, J. J. Zhu, Z. S. Liu, S. M. Zhang, H. Yang, U. Jahn, K. H. Ploog, *J. Crystal Growth* **2008**, *310*, 5266.

[64] T. Kolbe, A. Knauer, J. Enslin, S. Hagedorn, A. Mogilatenko, T. Wernicke, M. Kneissl, M. Weyers, *J. Crystal Growth* **2019**, *526*, 125241.

[65] J. Hakamata, Y. Kawase, L. Dong, S. Iwayama, M. Iwaya, T. Takeuchi, S. Kamiyama, H. Miyake, I. Akasaki, *Phys. Status Solidi B* **2018**, *255*, 1700506.

[66] N. Nepal, M. L. Nakarmi, J. Y. Lin, H. X. Jiang, *Appl. Phys. Lett.* **2006**, *89*, 092107.

[67] M. Bickermann, B. M. Epelbaum, O. Filip, P. Heimann, S. Nagata, A. Winnacker, *Phys. Status Solidi B* **2009**, *246*, 1181.

[68] Q. Yan, A. Janotti, M. Scheffler, C. G. Van de Walle, *Appl. Phys. Lett.* **2014**, *105*, 111104.

1901022 (11 of 11)